

Zeeman Effect, Polarization, and Selection Rules of $\text{Sm}^{2+}:\text{K}^+$ Vacancy Pair Fluorescence in $\text{KCl}\dagger$

FRANCIS K. FONG

North American Aviation Science Center, Thousand Oaks, California

AND

EUGENE Y. WONG

Department of Physics, University of California, Los Angeles, California

(Received 13 February 1967)

The fluorescence of Sm^{2+} ions in KCl has been studied at 4.2°K under a magnetic field of 26 kG. First- or second-order Zeeman effect has been observed in half of the observed emission lines. The anisotropy of the Zeeman effects has been observed in lines resulting from transitions between the 5D term and the 7F_4 , 7F_6 , and 7F_8 levels. On this basis, C_{4v} sites arising from K^+ vacancies oriented along the $\langle 100 \rangle$ axes and C_{2v} sites resulting from K^+ vacancies oriented along the $\langle 110 \rangle$ axes with respect to the Sm^{2+} ions have been positively identified. Polarization and selection rules of the $^5D_0 \rightarrow ^7F_J$ transitions have been deduced for C_{2v} and C_{4v} site symmetries. An effective spin Hamiltonian with $S=1$ has been employed to describe the Zeeman effect. The spin Hamiltonian for the identified C_{2v} site symmetry,

$$H_{\text{eff}} = g\beta\mathbf{H} \cdot \mathbf{S} + D[S_z^2 - \frac{1}{3}S(S+1)] + E(S_+^2 + S_-^2),$$

has a vanishing value for E and resembles that for the C_{4v} site symmetry. This is because the additional ligand field arising from the K^+ vacancy is axial.

I. INTRODUCTION

THE fluorescence of Sm^{2+} ions has been investigated by Dieke and Sarup,¹ who observed that the fluorescence spectrum of Sm^{2+} occurring as impurity in very small concentrations in LaCl_3 resembles in all details that of the isoelectronic ion Eu^{3+} . It was postulated that excitation occurs through the strong broad-band absorption to $4f^65d^1$ in the visible, which is followed by the transfer of energy to the 5D term of the $4f^6$ configuration, from which emission to components of the ground multiplet 7F is observed.

The absorption and emission spectra of Sm^{2+} in KCl and other alkali halide crystals have been investigated by Bron and co-workers.² All the J levels of the 7F term of the $4f^6$ configuration including the Stark levels of the $J=0, 1,$ and 2 levels were identified. Crystal-field parameters were calculated through a C_{2v} model. The absorption spectra at 10°K shows vibronic lines with Frank-Condon structure, indicative of $f-d$ transitions. Two vibrational frequencies were identified as due to localized oscillations of the SmCl_2 molecule with C_{2v} symmetry. While good agreement apparently exists between their experimental data and theoretical studies, two problems arise after a careful study of their works:

(1) The fluorescence spectrum identified as arising from Stark separation shows equal spacing for the 7F_1 and 7F_2 J levels, as shown in Table I. These equally spaced lines appear to be more like vibronic lines than Stark components. It should be possible to test the

Stark-splitting hypothesis by the observance of second-order Zeeman shifts, if any, with the application of an external magnetic field.

(2) The Sm^{2+} ion and its charge balance, the K^+ vacancy, can be oriented with respect to each other in a number of inequivalent ways. This is easily seen by visual inspection of the KCl lattice model. The existence of different site symmetries of paramagnetic divalent cations has been established by Schneider *et al.*³ and Watkins⁴ by electron spin resonance. It is therefore not clear why only one unique C_{2v} site was considered by Bron *et al.*² in their analyses of the Sm^{2+} spectra.

In an attempt to clarify the matter somewhat, we have made use of the fluorescence Zeeman effect in the study of ion-pairing in Sm^{2+} -doped KCl crystals. Like electron spin resonance, the fluorescence Zeeman effect provides us with a sensitive probe into the environment of the ion under study. Unlike electron spin resonance, it does not require a paramagnetic ground level, and, as in the present case, provides us with several J levels of the ground multiplet. In the following sections, we shall present *positive* identification of the C_{2v} and C_{4v} site symmetries by the fluorescence Zeeman effect, and by polarization studies. Evidence will also be presented which shows that complex association could extend considerably beyond the second-nearest neighbor.

II. THEORETICAL CONSIDERATIONS

The $[100]$, $[110]$, and $[111]$ axes of the KCl lattice are shown in Fig. 1. If the K^+ vacancy is situated along the $\langle 110 \rangle$ direction with the Sm^{2+} ion at the origin, the

[†] This research was supported in part by a grant from the National Science Foundation Grant No. GP 6183.

¹ G. H. Dieke and R. Sarup, *J. Chem. Phys.* **36**, 371 (1962).

² W. E. Bron and W. R. Heller, *Phys. Rev.* **136**, A1433 (1964); M. Wagner and W. E. Bron, *ibid.* **139**, A223 (1965); W. E. Bron and M. Wagner, *ibid.* **139**, A233 (1965).

³ E. E. Schneider and J. E. Caffyn, *Defects in Crystalline Solids* (The Physical Society, London, 1955), p. 74; P. A. Forrester and E. E. Schneider, *Proc. Phys. Soc. (London)* **B69**, 833 (1956).

⁴ G. D. Watkins, *Phys. Rev.* **113**, 79 (1959); 91 (1959).

site symmetry in C_{2v} . If the vacancy is along the $\langle 100 \rangle$ direction, the site symmetry will be C_{4v} . Similarly, if the vacancy is located anywhere along the $\langle 111 \rangle$ direction, the site symmetry will be C_{3v} . Vacancies in all other directions will give lower symmetries. It is obvious that not only different site symmetries exist, the same site symmetry has different orientations. In Fig. 2, the three equivalent C_{4v} sites and the six equivalent C_{2v} sites are shown.

For the C_{4v} site symmetry, three orientations exist along the $[100]$, $[010]$, and $[001]$ directions [Fig. 2(A)]. If the cubic crystal field is larger than that from the charge compensation, the wave functions from the Hamiltonian with cubic-crystal-field symmetry can be

TABLE I. Emission spectrum of KCl:Sm²⁺: (A) at 4.2°K by present authors, and (B) at 10°K by Bron and Heller (Ref. 2). Intensities are given by s=strong, m=medium, w=weak, and vw=very weak. The lines are given in Å.

	A	B		A	B
7F_0			7F_4		
s	6891.9	6892.8	m	8132.6	8134.0
w	6899.1		m	8194.7	8195.9
			m	8203.2	
7F_1					8206.4
s	7014.7	7015.6	s	8204.9	
w	7018.0				
vw	7018.7				
s	7031.7	7032.6			
s	7048.2	7049.2	7F_5		
			vw	8742.8	
7F_2			w	8746.4	
s	7264.4	7266.5	m	8747.3	8749.5
s	7282.8	7285.0	s	8778.4	8781.1
w	7285.0		s	8831.5	8834.2
w	7301.0		m	8845.2	8848.0
s	7304.6	7306.8			
w	7320.8				
w	7322.7		7F_6		
s	7327.6	7329.6	s	9439.1	9442.2
7F_3					
w	7666.1	7668.6	s	9440.0	
m	7667.5	7670.1	s	9451.9	
m	7671.4	7673.8	vw	9462.2	
m	7684.4	7686.9	vw	9503.3	9506.0
s	7693.5		vw	9515.0	9517.9
		7695.4	vw	9522.5	9525.9
s	7694.5				

considered as first-order solutions. The electric field due to the charge compensation and the external magnetic field will have an effective spin Hamiltonian in the form

$$H_{\text{eff}} = \beta \mathbf{H} \cdot \mathbf{g} \cdot \mathbf{S} + D[S_z^2 - \frac{1}{3}S(S+1)]. \quad (1)$$

Under cubic field, only the two 3-dimensional irreducible representations Γ_4 and Γ_5 will give rise to first-order Zeeman effect, since the operator \mathbf{S} transforms like Γ_4 , and the Kronecker product of the 2-dimensional representation Γ_3 with Γ_4 does not contain Γ_3 . The fictitious spin S will be 1, and the g factor is isotropic. If higher-order wave functions are used, such as those from the C_{4v} symmetry, the g tensor will be axial, and g_{11} is

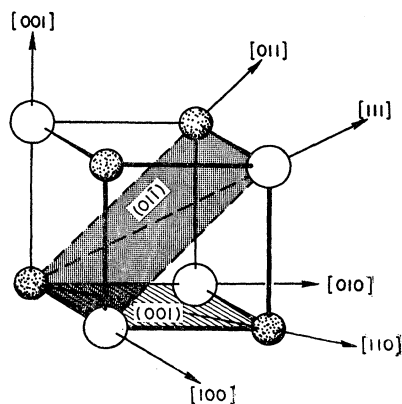


FIG. 1. The (001) and (011) planes of the KCl lattice with various crystal axes.

not the same as g_{\perp} . The second term in Eq. (1) represents the electric field due to the charge compensation, which splits the three-dimensional Γ_4 and Γ_5 representations into A_2+E , and B_2+E representations of C_{4v} symmetry, respectively. While electric-dipole transition from 5D_0 to E is allowed, those involving A_2 and B_2 states are forbidden according to group-theoretic arguments.

Within the manifold $S=1$, the Paschen-Back effect as well as the first-order Zeeman splitting will occur depending upon the orientation of the magnetic field \mathbf{H} with respect to the fourfold axis. In Fig. 2(A), the three different sites a , b , and c are shown with their fourfold axes along the $[100]$, $[010]$, and $[001]$ directions. When \mathbf{H} is in the $[100]$ direction, site a with its

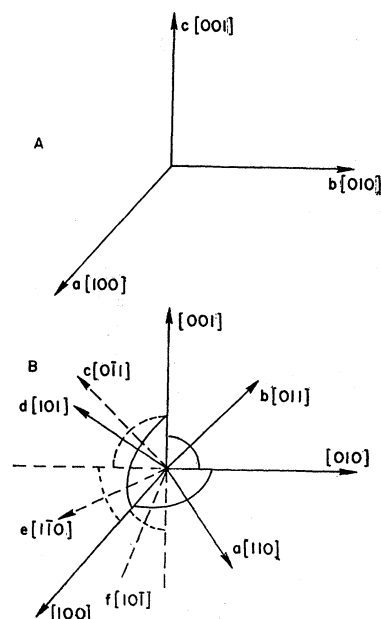


FIG. 2. Orientations of (A) C_4 axes of the three equivalent C_{4v} sites and (B) C_2 axes of the six equivalent C_{2v} sites.

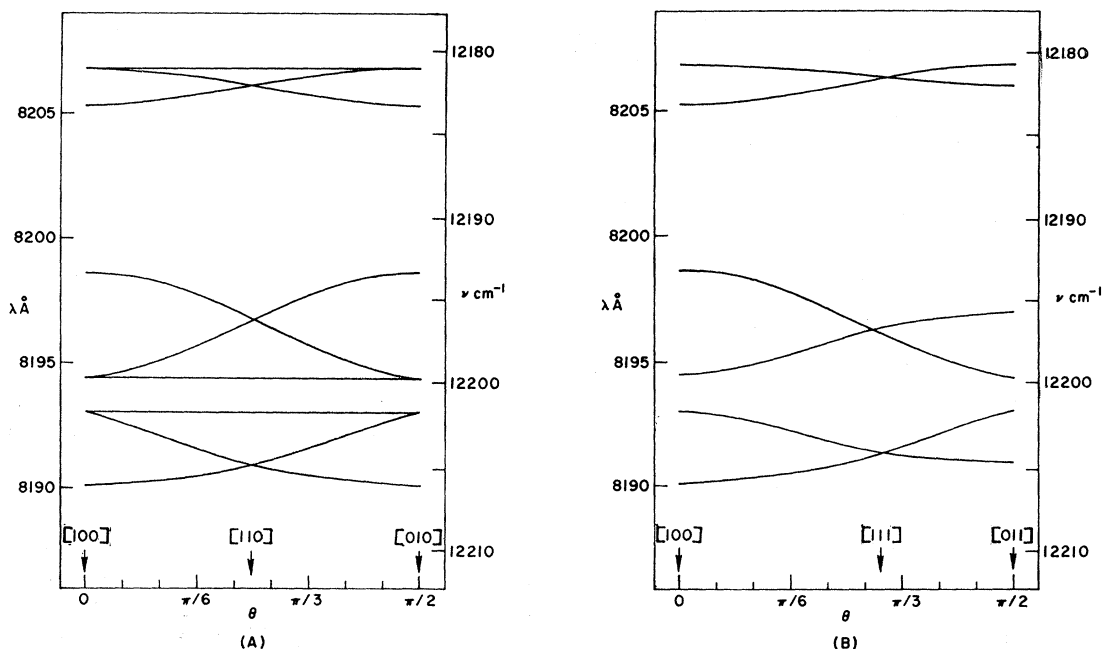


FIG. 3. Theoretical C_{4v} Zeeman anisotropy patterns with \mathbf{H} rotating in (A) the (001) plane and (B) the (01 $\bar{1}$) plane. Calculations were made with $g\beta H = 6.45 \text{ cm}^{-1}$ and $D = 16.24 \text{ cm}^{-1}$ employing the Hamiltonian (1). The scales in λ and ν are shown for comparison with the observed patterns shown in Fig. 7. The full pattern in the 8190.1–8198.6 Å region corresponds to the transitions ${}^5D_0 \rightarrow |M_s = \pm 1\rangle$ and the half-pattern at longer wavelengths corresponds to the forbidden transition ${}^5D_0 \rightarrow |M_s = 0\rangle$.

fourfold axis parallel to \mathbf{H} will give rise to first-order Zeeman splitting of the two complex-conjugate states to the extent of $2\beta gH$. Sites b and c are magnetically equivalent, and will only give rise to the Paschen-Back effect which occurs through the interaction of the $|M_s = 1\rangle$ and $|M_s = \bar{1}\rangle$ states with $|M_s = 0\rangle$. The no-field line associated with the E irreducible representation will thus give rise to a four-line pattern in the magnetic field. When the magnetic field is rotated away from the $[100]$ direction in the (001) plane (see Fig. 1), sites a , b , and c become nonequivalent, and a six-line pattern emerges without consideration of the selection rules (see Sec. V). When \mathbf{H} is along the $[110]$ direction, sites a and b are equivalent, and the six-line pattern merges into a four-line pattern. As \mathbf{H} is rotated to the $[010]$ direction, the Zeeman pattern makes a mirror image return to the initial four-line pattern.

When \mathbf{H} is rotated away from the $[100]$ direction in the (01 $\bar{1}$) plane (Fig. 2), sites b and c remain equivalent, and a maximum of four lines can be expected. When \mathbf{H} is in the $[111]$ direction, all three sites are equivalent, and only a two-line pattern is expected. Figures 3(A) and 3(B) show typical theoretical patterns with \mathbf{H} rotating in the (001) and (00 $\bar{1}$) planes, respectively, calculated from the effective Hamiltonian (1) with $g\beta H = 6.45 \text{ cm}^{-1}$ and $D = 16.24 \text{ cm}^{-1}$. The eigenstate $|M_s = 0\rangle$ will give rise to second-order Zeeman effect only, and is expected to show half of the patterns described for the two complex-conjugate states (Fig. 3).

The two-dimensional and one-dimensional irreducible representations of the cubic symmetry will have fictitious spins of $\frac{1}{2}$ and 0 for the above effective Hamiltonian, except that g will be zero, since these states are nonmagnetic so far as first-order perturbation is concerned.

In C_{2v} site symmetry, the pure electronic state has no degeneracy according to group theory. When the Sm^{2+} ion and the K^+ vacancy are nearest-neighbor complexes, two of the six nearest chloride ions are expected to undergo nonradial displacements about the impurity ion as the Sm^{2+} ion and the vacancy are displaced toward each other as a result of Coulomb attraction. For this model, the crystal field at the Sm^{2+} ion will be nonaxial, and all the degeneracies will be removed. This was the model employed by Bron and co-workers,² in which case the effective spin Hamiltonian will take the form

$$H_{\text{eff}} = \beta \mathbf{H} \cdot \mathbf{g} \cdot \mathbf{S} + D[S_z^2 - \frac{1}{3}S(S+1)] + E(S_+^2 + S_-^2). \quad (2)$$

If, on the other hand, the vacancy is sufficiently far away that the cubic environment of the Sm^{2+} ion is retained and that the potential at the Sm^{2+} ion due to the vacancy and the distortion around it appears to be that due to a point charge, this additional ligand field will be axial. Equation (2) now reduces to the spin Hamiltonian in Eq. (1), since $E = 0$ for axial symmetry. The first-order, as well as the second-order Zeeman effect will be possible, just as in the case of C_{4v} site

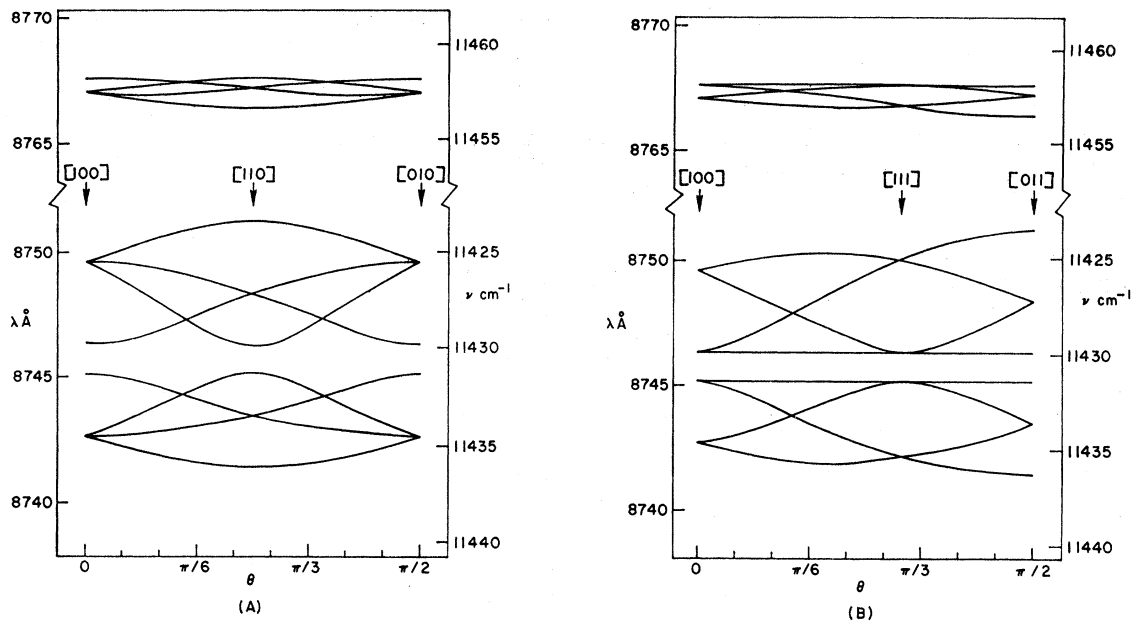


FIG. 4. Theoretical C_{2v} Zeeman anisotropy patterns with \mathbf{H} rotating in (A) the (001) plane and (B) the (01 $\bar{1}$) plane. Calculations were made with $g\beta H = 6.40 \text{ cm}^{-1}$ and $D = 28.15 \text{ cm}^{-1}$ employing the Hamiltonian (1). The scales in λ and ν are shown for comparison with the observed patterns shown in Fig. 8. The half-pattern at long wavelengths corresponds to the forbidden transition ${}^5D_0 \rightarrow |M_s = 0\rangle$, and the full pattern is associated with the transitions ${}^5D_0 \rightarrow |M_s = \pm 1\rangle$.

symmetry. Indeed, much of the above discussion for the C_{4v} case can be applied to the present case, except that the patterns for the anisotropy of the Zeeman effect will be more complicated, since there are six orientations of the twofold axes along the $[110]$, $[011]$, $[0\bar{1}1]$, $[101]$, $[1\bar{1}0]$, and $[10\bar{1}]$ directions. The six equivalent sites a , b , c , d , e , and f are shown in Fig. 2(B).

Consider the transition ${}^5D_0 \rightarrow |M_s = \pm 1\rangle$. When the magnetic field \mathbf{H} is in the $[100]$ direction, four (a , d , e , and f) of the six sites are magnetically identical, and are inequivalent to the two sites (b and c) with their C_2 axes along the $[011]$ and $[0\bar{1}1]$ directions, which are themselves identical to each other. The two complex-conjugate states will thus give rise to four lines. The separation of the two closer lines gives the extent of the second-order Zeeman effect. As \mathbf{H} is rotated away from the $[100]$ direction in the (001) plane (Fig. 1), the two sites d and f with their C_2 axes along $[101]$ and $[10\bar{1}]$ remain magnetically identical as well as the sites b and c with their C_2 axes along the $[011]$ and $[0\bar{1}1]$ directions. Sites a and e differ magnetically from each other as well as from all the other C_{2v} sites. An eight-line pattern thus emerges. When \mathbf{H} is in the $[110]$ direction, sites b , c , d , and f with their C_2 axes along the $[011]$, $[0\bar{1}1]$, $[101]$, and $[10\bar{1}]$ directions become identical, and a six-line pattern is expected. As \mathbf{H} rotates from the $[110]$ direction to the $[010]$ direction, the pattern makes a mirror-image return to the four-line pattern of the initial orientation of \mathbf{H} in the $[100]$ direction.

When the magnetic field rotates away from the $[100]$ direction in the (01 $\bar{1}$) plane, sites a and d are identical as well as sites e and f . Sites b and c differ from each other and from the other four C_{2v} sites. An eight-line pattern thus results. When \mathbf{H} is in the $[111]$ direction, sites a , b , and d become identical as well as sites c , f , and e . A four-line pattern thus results. Rotation of \mathbf{H} away from the $[111]$ direction in the (01 $\bar{1}$) plane again causes an eight-line pattern which eventually merges into a six-line pattern as \mathbf{H} is oriented in the $[011]$ direction. The curves of the calculated anisotropic Zeeman effect as \mathbf{H} rotates in the (001) and (01 $\bar{1}$) planes are shown in Fig. 4. The values $g\beta H = 6.40 \text{ cm}^{-1}$ and $D = 28.15 \text{ cm}^{-1}$ were employed in the calculations.

To our surprise, no C_{3v} site symmetries have been observed. We shall therefore omit theoretical discussion on complexes oriented along the $\langle 111 \rangle$ axes.

III. EXPERIMENTAL METHODS

The growth of Sm²⁺-doped single KCl crystals and the methods of quantitative analysis of the Sm²⁺ content in these crystals have been described previously.⁵ The samples employed for the present studies contained approximately 3.6×10^{18} Sm²⁺ ions cm^{-3} . In accordance with previous authors,² the samples were quenched from elevated temperatures in order to avoid aggregate formations.

The emission and absorption spectra were measured with a 20-m Baush & Lomb grating (4 in. by 4 in.

⁵ F. K. Fong, J. A. Cape, and E. Y. Wong, Phys. Rev. **151**, 299 (1966).

15 000-per-in. grating) spectrograph at liquid-helium temperature. The wavelengths were calibrated by the spectrum of iron arc. The results can be reproduced to an average deviation of 0.1 Å for most of the strong sharp lines, but for the broad weak lines, the deviation can be up to 0.3 Å. The spectra were taken with a 100-W tungsten projector lamp, and a red cutoff filter was used for the fluorescence spectrum.

The Zeeman effect was observed with a 10-in. magnet with a gap of 1-in. The magnetic field was calibrated by the emission spectrum of Hg, and also by Hall probe which was calibrated by NMR. The measurement of the magnetic field can be reproduced to only 1% by the two methods.

Polarization studies were made with a Wallensten prism. Measurements were made with the magnetic field in the [100] direction and in the [110] direction. The emission was viewed 90° away from the magnetic field in the (001) plane.

IV. EXPERIMENTAL RESULTS AND INTERPRETATION: ZEEMAN EFFECT AND SITE SYMMETRIES

The results of an emission spectrum of medium exposure are shown in Table I together with the spectrum reported by Bron and Heller. Except for a few deviations, we have reproduced the Bron-Heller spectrum. Actually, many more lines have been observed in our strong exposures, as shown in Fig. 5. Our attention, however, will be focussed on the lines observed with medium exposures, since they are more appropriate for comparison with those of the previous work.² The results may be most logically presented in the order of ascending J values for the 7F components, as is done in the following.

7F_0 , 7F_1 , and 7F_2

The lines associated with $J=0, 1$, and 2 of the 7F term appear as narrow lines in the region of 6850–7350 Å. The strong lines listed in Table I were identified by Bron and Heller² as Stark components of the three J levels. If this interpretation is correct, it should be possible to predict the magnitude of the second-order Zeeman effect. By using Bron and Heller's crystal-field parameters, we have calculated the second-order Zeeman effect for the 7F_2 and 7F_1 . For the 7F_2 level, there are calculated shifts of 0.084, -0.084 , 0.41, -0.22 , and -0.19 cm^{-1} for the five calculated Stark states at 13 808.6, 13 741.6, 13 713, 13 680.2, and 13 675.8 cm^{-1} when a magnetic field of 27 000 G is applied along the twofold axis of the C_{2v} site. The 7F_1 level has the same order of shift. Figure 6 shows the result taken at second order with a resolving power of 10^5 . The top and bottom exposures of the Hartman diaphragm were taken without an applied magnetic field, and the center position was taken with a magnetic field of 27 000 G along the [110] direction. No Zeeman

effect was detected. The limit of the detection is dependent on the linewidth. For the four lines at 7264.4, 7282.8, 7304.6, and 7327.6 Å the widths are 0.5, 0.2, 0.5, 0.8 cm^{-1} , respectively. If one considers that the center of the edges of a line can be detected to $\frac{1}{10}$ of the width, the limitation of the detection is 0.1 cm^{-1} for the broadest line. Since the maximum calculated shift with the Bron-Heller model is 0.41 cm^{-1} , their identification of the Stark components appears to be incorrect. Also, with our much better resolving power, the line at 7264.4 Å does not show any doublet structure, which is further evidence against their interpretation.²

The three lines at 7014.7, 7031.7, and 7048.2 Å have about the same separation (~ 37 cm^{-1}) as those at 7282.8, 7304.6, and 7327.6 Å, which is most likely of vibronic origin.⁶ The lines become increasingly broader as the wavelength increases. Two similar patterns are observed in the absorption spectrum.⁶

The fact that the vibrational frequency (~ 37 cm^{-1}) does not change appreciably in going from KCl to KBr as the host² has led to the model⁶ in which localized vibrations involve only motion of the Sm^{2+} ion.

In sum, the lines at 7014.7, 7264.4, and 7282.8 Å are believed to be of electronic origin. The two lines at 7031.7 and 7048.2 Å and those at 7304.6 and 7327.6 Å are of vibronic origin. It is not clear whether or not the lines at 7264.4 and 7282.8 Å originate from the same Sm^{2+} ion. Most likely, these lines are emitted from ions at C_{2v} sites, with Stark splitting in the order of 10^2 cm^{-1} resulting in no detectable Zeeman effect.

7F_3

The lines associated with $J=3$ of the 7F term appear in the region 7675–7705 Å. Zeeman effect is observed in

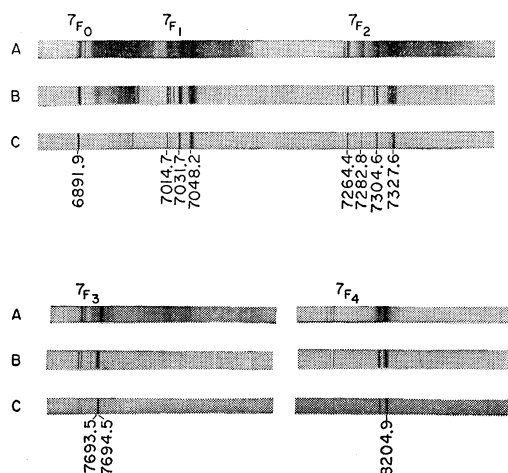


Fig. 5. Spectral lines of ${}^5D_0 \rightarrow {}^7F_0$, 7F_1 , 7F_2 , 7F_3 , and 7F_4 of three different exposures: (A) 50- μ slit, 40 min; (B) 20- μ slit, 10 min and (C) 10- μ slit, 2 min. (compare with Table I).

⁶ F. K. Fong and E. Y. Wong, in *Proceedings of Conference on Optical Properties of Ions in Crystals* (John Wiley & Sons, Inc., New York, to be published).

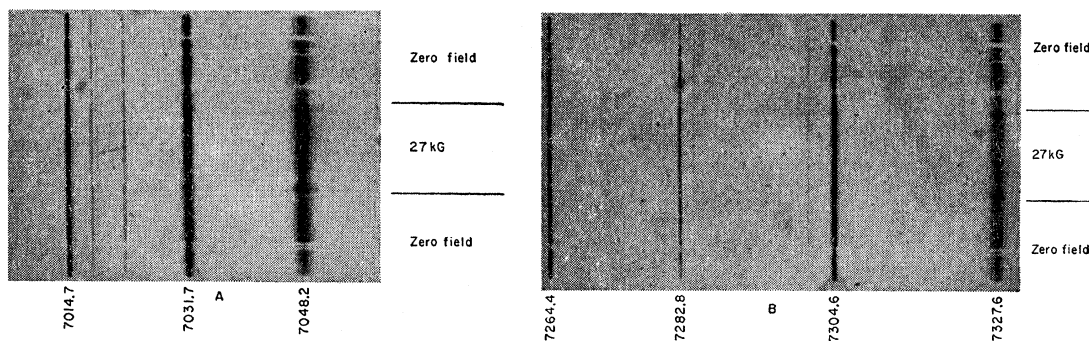


FIG. 6. Three exposures of the (A) 7F_1 and (B) 7F_2 spectral lines. The top and bottom exposures of the Hartman diaphragm were made at zero field, and the center exposure was made with a magnetic field of 27 000 G along the $[110]$ direction.

several lines, but no recognizable patterns of anisotropy can be definitively identified. The patterns observed in the proximities of 7671, 7693, and 7695 Å give incomplete C_{4v} patterns with both isotropic lines missing [see Fig. 3(A)] when the magnetic field is rotated in the (001) plane. The pattern that originates from the line at 7684 Å is not understood, nor is the pattern resolved with the grating operating in second order for the group of lines at 7694 Å. Clearly, further work is necessary for the identification of the sites responsible for these patterns. A more detailed presentation of the data must therefore be postponed to a future date.

7F_4

The lines associated with 7F_4 occur in the region 8120–8210 Å. Under an external magnetic field \mathbf{H} , most of the observed lines show a first- or second-order

Zeeman effect, the angular variations of which, with \mathbf{H} rotating in the (001) and (01 $\bar{1}$) planes, are shown in Fig. 7(a) and 7(b), respectively. Immediately obvious is the C_{4v} pattern originating from the no-field line at 8194.6 Å. Less apparent are two more C_{4v} patterns which arise from the no-field lines at 8203.2 and 8204.9 Å. Consider the pattern arising from the no-field line at 8194.6 Å with \mathbf{H} rotating in the (001) plane [Fig. 7(A)]. The solution of the 3-dimensional spin-Hamiltonian matrix when \mathbf{H} is perpendicular to the c axis gives a line at the zero-field position, and can be used as a check on the validity of the spin Hamiltonian [Eq. (1)]. This was observed experimentally. The two lines at maximum separation corresponding to $|M_s=1\rangle$ and $|M_s=\bar{1}\rangle$ when \mathbf{H} is parallel to the C_4 axis should be symmetrically displaced about the no-field line as required by the solution of the spin-Hamiltonian

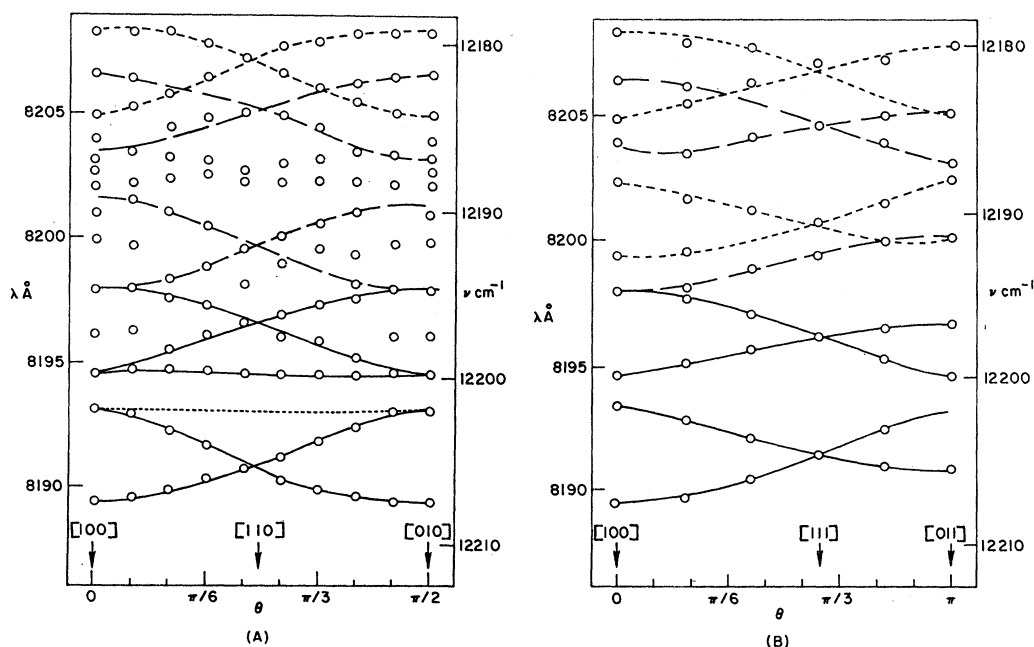


FIG. 7. Observed C_{4v} Zeeman anisotropy patterns of 7F_4 lines with (A) \mathbf{H} rotating in the (001) plane, and (B) \mathbf{H} rotating in the (01 $\bar{1}$) plane.

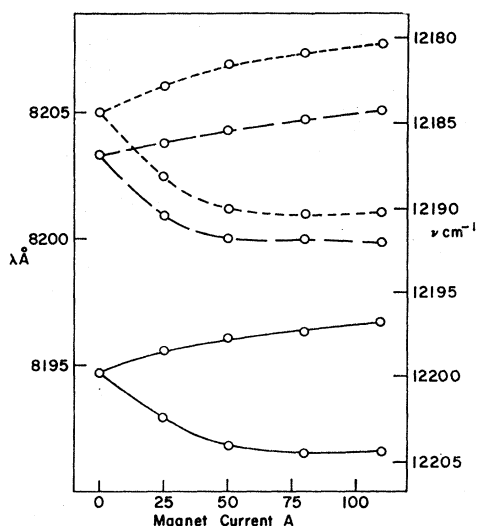


FIG. 8. Field dependence of the Zeeman splittings of three 7F_4 no-field lines at 8194.6, 8203.2, and 8204.9 Å with \mathbf{H} along the $[111]$ direction.

matrix. That this is the case is exemplified by the calculated C_{4v} pattern shown in Fig. 3(A), for which the parameters $g\beta H = 6.45 \text{ cm}^{-1}$ and $D = 16.24 \text{ cm}^{-1}$ from the experimental C_{4v} pattern originating from the 8194.6 Å no-field line [Fig. 7(A)] have been employed in the calculations. This, however, was not confirmed experimentally [compare Fig. 7(A) with Fig. 3(A),] which suggests second-order effects due to interaction of the $|M_s = 1\rangle$ and $|M_s = \bar{1}\rangle$ states with energy states lying outside the $S = 1$ manifold. The missing of the isotropic line at 8193.2 Å [Fig. 7(A)] is due to selection rules, which will be elaborated in Sec. V. For the observed C_{4v} pattern due to the 8194.6 Å line, $g = 5.04$. For

the other two patterns corresponding to the no-field lines at 8203.2 and 8204.9 Å, g values of 5.34 and 5.50, respectively, have been obtained. For $J = 4$, the calculated values for g in cubic representation are 0.75 and 3.75 for Γ_4 and Γ_6 , respectively. The rather large experimental g values thus suggest that the three groups of C_{4v} patterns arise from transitions involving the irreducible representations Γ_6 . Anisotropy patterns observed in the spectral region 8120–8130 Å for the much weaker lines do not give definitive patterns, and will not be discussed at the present.

When the external magnetic field is directed along the $[111]$ axis, each of the three no-field lines at 8194.6, 8203.2, and 8204.9 Å splits into two lines. This is consistent with the fact that all three sites, a , b , and c [Fig. 2(A)], are magnetically equivalent. The field dependence of the splittings is shown in Fig. 8.

7F_5

The lines associated with 7F_5 occur in the region 8739–8790 Å, of which the lines in the proximity of 8799 Å are not well resolved. Most notable is the Zeeman anisotropy pattern arising from the no-field line at 8746.5 Å with \mathbf{H} rotating in (001) and $(01\bar{1})$ planes, as shown in Figs. 9(A) and 9(B). For $S = 1$, the pattern arising from the 8746.5 Å line can be readily explained in terms of the first- and second-order Zeeman splittings of the states $|M_s = 1\rangle$ and $|M_s = \bar{1}\rangle$ for the case of C_{2v} symmetry, in which the crystal field is axial (Sec. II). The theoretical patterns shown in Figs. 4(A) and 4(B) were calculated with experimental parameters $g\beta H = 6.40 \text{ cm}^{-1}$ and $D = 28.15 \text{ cm}^{-1}$, measured from the data presented in Figs. 9(A) and 9(B). The effective Hamiltonian given in Eq. (1) was employed with \mathbf{H} rotating in the (001) and $(01\bar{1})$ planes. The favorable compari-

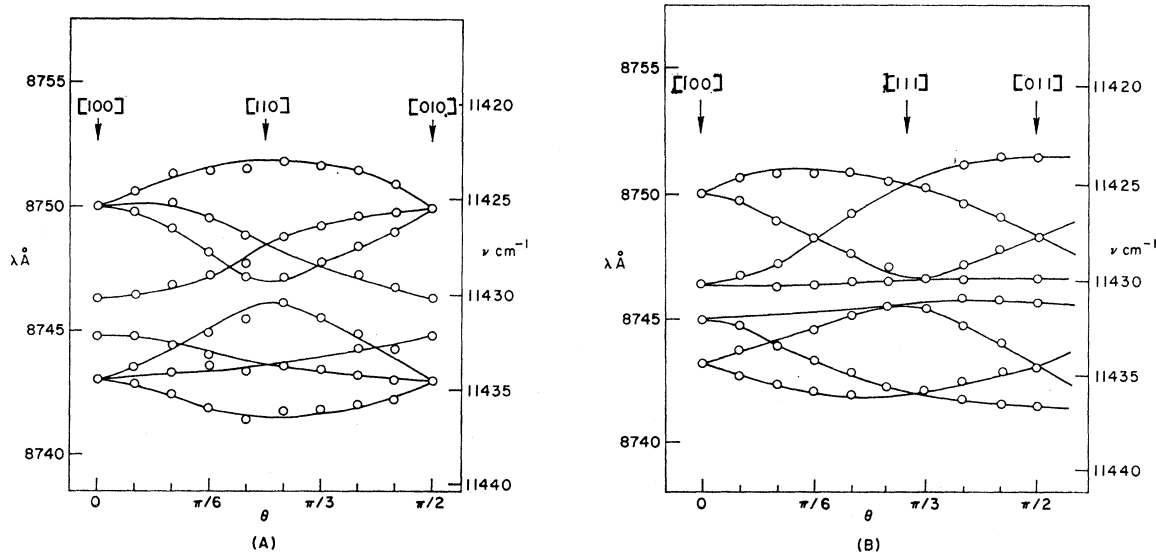


FIG. 9. Observed C_{2v} Zeeman anisotropy patterns arising from the no-field line at 8746.5 Å (7F_5) with (A) \mathbf{H} rotating in the (001) plane, and (B) \mathbf{H} rotating in the $(01\bar{1})$ plane.

son of these theoretical patterns with experimental observations (Figs. 4 and 9) suggests strongly the existence of C_{2v} sites with the K⁺ vacancy sufficiently removed from the Sm²⁺ ion as not to affect appreciably its immediate cubic environment. This is to be distinguished from the C_{2v} model assumed by Bron *et al.*²

7F_6

The lines associated with 7F_6 occur in the region 9431–9525 Å. Here the no-field spectrum shows two closely spaced lines at 9439.16 and 9439.95 Å. Upon the application of an external magnetic field, Zeeman splitting of these two lines becomes evident. The anisotropy of the Zeeman effects with H rotating in the (001) and (01 $\bar{1}$) planes is shown in Figs. 10(A) and 10(B). The zero-field splitting indicates the mixing of $|M_s=1\rangle$ and $|M_s=\bar{1}\rangle$ due to distortion of the cubic lattice, in which case it is necessary to employ the effective Hamiltonian shown in Eq. (2). From the

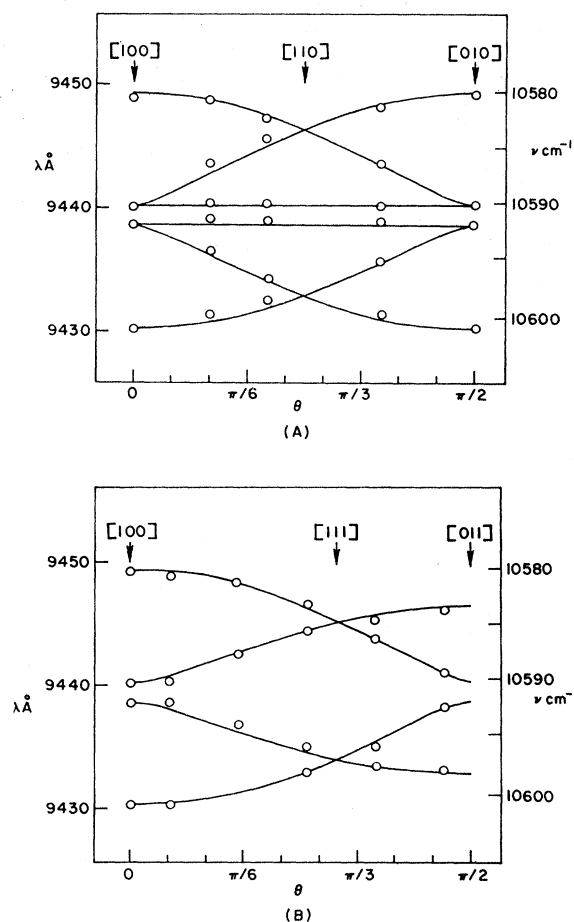


FIG. 10. C_{4v} Zeeman anisotropy patterns arising from the two zero-field lines at 9439.16 and 9439.95 Å of 7F_6 with (A) H rotating in the (001) plane, and (B) H rotating in the (01 $\bar{1}$) plane. The circles are experimental points and the solid lines represent theoretical calculations made with $g=8.57$, $D=132.04 \text{ cm}^{-1}$, $E=0.25 \text{ cm}^{-1}$, and $H=26\,000 \text{ G}$ employing the Hamiltonian (2).

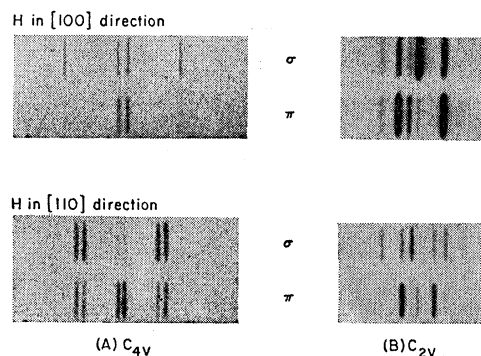


FIG. 11. Polarized spectra of (A) 7F_6 and (B) 7F_6 lines taken with the magnetic field in the [100] and [110] directions and the emission observed 90° away from H in the (001) plane.

experimental points, the values 8.57, 132.04, and 0.25 cm^{-1} have been obtained for the parameters g , D , and E , respectively. The theoretical patterns calculated with these values for the three equivalent C_{4v} sites a , b , and c are superimposed upon the experimental points in Fig. 10. The agreement is excellent.

Because of the mixing of the two complex-conjugate states, both isotropic lines have been observed in the Zeeman anisotropy pattern with H rotating in the (001) plane. This is to be compared with that observed in the case of 7F_4 , in which only the isotropic line coinciding with the zero-field line has been observed. Noteworthy is the fact that despite the zero-field splitting, the experimental C_{4v} patterns in the case of 7F_6 are more nearly ideal than those in the case of 7F_4 .

V. POLARIZED EMISSION AND SELECTION RULES

Polarized spectra taken with the magnetic field H in the [100] and [110] directions and the emission observed 90° away from H in the (001) plane are shown for the two groups of lines associated with the C_{4v} site (7F_6) and the C_{2v} site (7F_6) in Fig. 11. Here σ polarization signifies $E \perp H$, whereas π polarization denotes $E \parallel H$. No polarization effects have been observed for the lines associated with the three lowest J levels 7F_0 , 7F_1 , and 7F_2 , whereas those observed in the case of 7F_3 and 7F_4 are complicated by overlapping patterns.

It is possible, from group-theoretic considerations, to determine from the polarization patterns whether the transitions are of electric-dipole or magnetic-dipole origin. To do this, it is necessary to know the symmetries of the sites responsible for the spectral lines, the transformation properties of the eigenstates involved in the transitions, and those of the operator which connects these states. A transition between the initial state Ψ_i and the final state Ψ_f via the operator O is allowed if the matrix element $\langle \Gamma_i | \Gamma_0 | \Gamma_f \rangle$ is nonvanishing. This will be the case if Γ_0 is contained in the direct product of $\Gamma_i \times \Gamma_f$. Selection-rule tables can thus be constructed from character tables of the appropriate

Electric Dipole		
C_s	C_2	C_4
Γ_1 Γ_2	Γ_1 Γ_2	Γ_1 Γ_2 Γ_3 Γ_4
Γ_1 σ π	Γ_1 π σ	Γ_1 π σL σR
Γ_2 π σ	Γ_2 σ π	Γ_2 π σR σL
		Γ_3 σR σL π
		Γ_4 σL σR π

Magnetic Dipole		
C_s	C_2	C_4
Γ_1 Γ_2	Γ_1 Γ_2	Γ_1 Γ_2 Γ_3 Γ_4
Γ_1 σ π	Γ_1 σ π	Γ_1 σ πL πR
Γ_2 π σ	Γ_2 π σ	Γ_2 σ πR πL
		Γ_3 πR πL σ
		Γ_4 πL πR σ

FIG. 12. Selection-rule tables of the C_2 , C_s , and C_4 groups for electric-dipole and magnetic-dipole transitions. For the C_4 selection-rule tables, σR , σL , πR , and πL correspond to the operators $x+iy$, $x-iy$, L_x+iL_y , and L_x-iL_y , respectively.

symmetry groups,⁷ and these are given in Fig. 12 for the C_4 , C_2 , and C_s groups which will be involved in the ensuing discussions. The symbol σ or π in these tables indicates whether the \mathbf{E} vector is perpendicular or parallel to the z axis which is chosen to coincide with the direction of the magnetic field.

The theoretical σ and π polarized spectra of the C_{4v} and C_{2v} $\text{Sm}^{2+}:\text{K}^+$ vacancy pairs for electric-dipole and magnetic-dipole transitions with 5D_0 as the initial state (Fig. 13) can be deduced as follows.

C_{4v} Site Symmetry

Under an external magnetic field \mathbf{H} , the three C_{4v} sites a , b , and c [Fig. 2(A)] become magnetically inequivalent. When \mathbf{H} is in the $[100]$ direction, the symmetry of site a is lowered to C_4 , whereas that of b or c is lowered to C_s . This can be seen by replacing \mathbf{H} by a current loop which destroys all symmetry properties except, for site a , the C_4 rotation axis along $[100]$ and, for sites b or c , the reflection plane (100) . Now the initial state 5D_0 transforms like the identity representation Γ_1 . For electric-dipole transitions, the components of the operator \mathbf{O} have the transformation properties of x , y , and z . Since, in C_4 symmetry, $|M_s=1\rangle$ and $|M_s=\bar{1}\rangle$ of the $S=1$ manifold transform like Γ_3 and Γ_4 , respectively, and $x+iy$ and $x-iy$, form the basis for these two irreducible representations, the $|M_s=\pm 1\rangle$ states of site a will give rise to two σ polarized lines separated by $2g\beta H$ (\mathbf{H} being parallel to the C_4 axis). For the two C_s sites b and c , $|M_s=1\rangle+|M_s=\bar{1}\rangle$ and $|M_s=1\rangle-|M_s=\bar{1}\rangle$ transform like Γ_1 and Γ_2 , respectively. For electric-dipole transitions, therefore, they should give rise to one σ polarized line and one π polar-

ized line (see selection table for C_s in Fig. 12), the latter of which coincides with the no-field line.

When \mathbf{H} is in the $[\bar{1}10]$ direction, the symmetry of site a or b is lowered to C_1 with no selection rules, resulting in $\sigma\pi$ polarization. The site symmetry of c is C_s . As before, the complex-conjugate states $|M_s=1\rangle+|M_s=\bar{1}\rangle$ and $|M_s=1\rangle-|M_s=\bar{1}\rangle$, transforming like Γ_1 and Γ_2 of the C_s group, will give rise to either σ or π polarization. The σ polarized line, however, has no intensity, since the corresponding oscillating dipole is oriented along the light-propagation vector (i.e., along $[\bar{1}10]$). This accounts for the missing isotropic line in the C_{4v} Zeeman anisotropy pattern observed in 7F_4 as discussed in Sec. IV.

The polarized spectra for magnetic-dipole transitions (Fig. 13) can be deduced with the aid of the selection-rule tables (Fig. 12) in a similar fashion. A detailed discussion is therefore omitted.

C_{2v} Site Symmetry

Consider the six C_{2v} sites a , b , c , d , e , and f [Fig. 2(B)]. When \mathbf{H} is in the $[100]$ direction, the symmetry of sites a , d , e , and f is lowered to C_1 , resulting in $\sigma\pi$ polarization. Sites b and c have C_s symmetry. Their complex-conjugate states, accordingly, will give rise to one σ polarized line and one π polarized line, the latter coinciding with the no-field line.

With \mathbf{H} in the $[\bar{1}10]$ direction, site a possesses C_2 symmetry. Here, $|M_s=1\rangle+|M_s=\bar{1}\rangle$ and $|M_s=1\rangle-|M_s=\bar{1}\rangle$ both transform like Γ_2 of the C_2 group, result-

	Electric Dipole	Magnetic Dipole
C_{4v}	H in $[100]$ direction	σ
	a b,c a	b,c a
	b	a b
	H in $[\bar{1}10]$ direction	π
	a,b c a,b	a,b c a,b
	σ	π
	a,b c a,b	a,b c a,b
C_{2v}	H in $[100]$ direction	σ
	a,d b a,d	a,d b a,d
	e,f c e,f	e,f c e,f
	π	π
	a,d b a,d	a,d b a,d
	e,f c e,f	e,f c e,f
	σ	π
	a b,c e b,c a	a b,c e b,c a
	d,f d d,f d	d,f d d,f d
	Zero field line	Zero field line

FIG. 13. Theoretical σ and π polarized spectra of electric-dipole and magnetic-dipole transitions between 5D_0 and $|M_s=\pm 1\rangle$ or $|M_s=1\rangle\pm|M_s=\bar{1}\rangle$ states for C_{4v} and C_{2v} site symmetries. The sites (corresponding to Fig. 2) responsible for the lines are indicated by the letters a , b , c , d , e , and f .

⁷ R. A. Satten, Hughes Research Laboratories Research Report No. 207, 1961 (unpublished).

ing in, for electric-dipole transitions, two pure σ polarized lines (C_2 selection-rule table, Fig. 12) separated by $2g\beta H$. Sites c , b , d , and f have C_1 symmetry with $\sigma\pi$ polarization. Site e , with its C_s symmetry, is expected to give rise to one σ polarized line and one π polarized line (see Fig. 13).

C_{2v} polarization patterns for magnetic-dipole transitions can be readily deduced in an analogous manner, and are shown in Fig. 13.

Comparison of the theoretical deductions (Fig. 13) and experimental observations (Fig. 11) readily reveals that the transitions under consideration are of electric-dipole origin. Discrepancies, however, do exist between theory and experiment. The observation of the two closely spaced lines in both σ and π polarized spectra of 7F_6 [corresponding to the observation of both isotropic lines in Fig. 10(A)] is suggestive of lattice distortions (Sec IV). The splitting of the two $\sigma\pi$ lines of 7F_6 with \mathbf{H} in the $[110]$ direction is due to a slight misalignment of the $[110]$ axis with the magnetic field, in which case sites a and b are no longer equivalent. More puzzling is the one discrepancy between theory and experiment in the case of 7F_5 (C_{2v}) polarization with \mathbf{H} in the $[110]$ direction. The observed σ and π polarized lines due to site e are reversed in position to those of the theoretical lines.

VI. CONCLUSION

The Zeeman effect observed in the KCl:Sm²⁺ fluorescence give positive identification of several types of Sm²⁺:K⁺ vacancy pairing. K⁺ vacancies located along the $\langle 100 \rangle$ axes will give rise to C_{4v} sites. The C_{4v} Zeeman anisotropy patterns associated with the three no-field lines at 8194.6, 8203.2, and 8204.9 Å have g values of 5.04, 5.34, and 5.50, respectively (see discussion on 7F_4). The C_{4v} pattern associated with the two closely spaced no-field lines at 9439.16 and 9439.95 Å (7F_6) gives $g=8.57$, $D=132.04$ cm⁻¹, and $E=0.25$ cm⁻¹, which is to be compared with the values $D=16.24$ cm⁻¹ and $E=0$ cm⁻¹ for the C_{4v} pattern originating from the 7F_4 line at 8194.6 Å. These four different C_{4v} patterns indicate the presence of at least four different C_{4v} Sm²⁺:K⁺ vacancy pairs probably with different distances of separation of the Sm²⁺ ions from the K⁺

vacancies. The C_{2v} pattern observed in 7F_5 arises from compensation of the Sm²⁺ ion by a K⁺ vacancy located along the $\langle 110 \rangle$ axes. Here the K⁺ vacancy is sufficiently far away from the Sm²⁺ ion that the immediate environment of the Sm²⁺ ion remains cubic. These C_{2v} Sm²⁺:K⁺ vacancy pairs are to be contrasted with the C_{2v} nearest-neighbor pairs, for which no first-order Zeeman effect should be possible. Sm²⁺ ions with non-axial C_{2v} or lower site symmetries will give rise only to second-order Zeeman effects. If the crystal-field Stark splitting of these low symmetry sites is of the order of 10² cm⁻¹, the second-order Zeeman effect will be small, and in most cases will be beyond the detection limit. For approximately half of the observed Sm²⁺ lines, no Zeeman effect has been observed.

From polarized spectra of the KCl:Sm²⁺ emission in an applied magnetic field, the transitions have been determined to be of electric-dipole origin. This has been done with a prior knowledge of the site symmetries of the Sm²⁺:K⁺ vacancy pairs responsible for the spectral lines considered.

Numerous problems remain for future investigation. The Zeeman anisotropy patterns observed for the 7F_3 lines have not been successfully accounted for. The reversal in position of the observed σ and π polarized lines also requires further clarification. Also complicating the situation are the possibilities of (1) charge compensation of the Sm²⁺ ions by O²⁻ ions and (2) aggregate formation of Sm²⁺ ions. These two aspects may be investigated by intentional contamination of the samples by O²⁻ ions and by increasing the Sm²⁺ doping concentrations, respectively. Finally, the deviation of the observed C_{4v} patterns from the ideal behavior suggests second-order effects due to interaction of the $|M_s=1\rangle$ and $|M_s=\bar{1}\rangle$ states with states lying outside the $S=1$ manifold (see discussion on 7F_4). More refined theoretical considerations, therefore, are necessary for a better understanding.

ACKNOWLEDGMENTS

We are grateful to J. Mohl for the growth of single crystals, and to P. Romo for the ethylene-diamine tetra-acetic acid analysis of the Sm content in the samples.

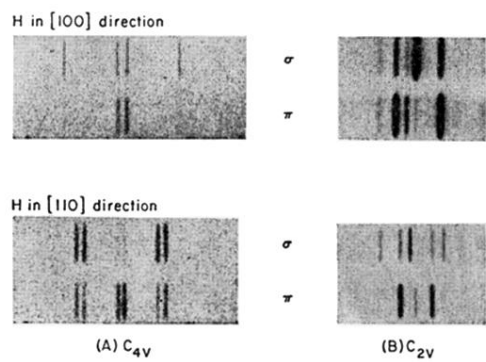


FIG. 11. Polarized spectra of (A) 7F_6 and (B) 7F_5 lines taken with the magnetic field in the $[100]$ and $[110]$ directions and the emission observed 90° away from \vec{H} in the (001) plane.

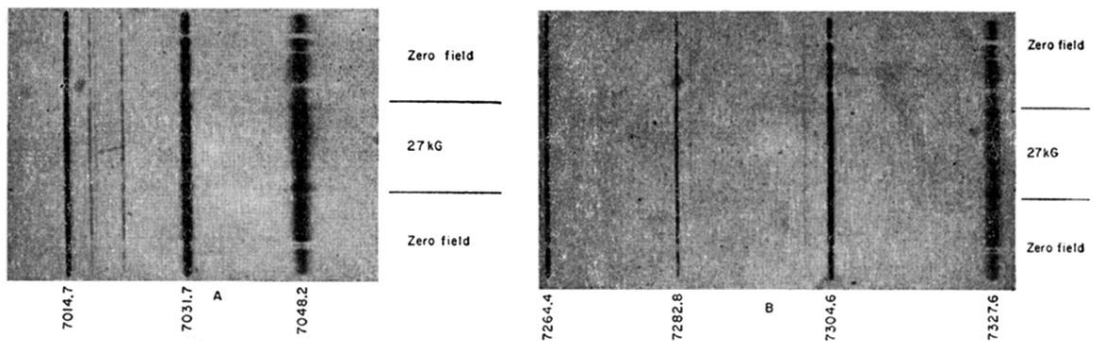


FIG. 6. Three exposures of the (A) 7F_1 and (B) 7F_2 spectral lines. The top and bottom exposures of the Hartman diaphragm were made at zero field, and the center exposure was made with a magnetic field of 27 000 G along the [110] direction.